Journal of
Materials Chemistry A

Materials for energy and sustainability

Accepted Manuscript

Journal of
Materials Chemistry A

Materials for energy and sustainability

rsc.li/materials-a

Volume 6
Number 12
28 March 2018
Pages 4883-5230

ISSN 2050-7488

ROYAL SOCIETY OF CHEMISTRY

COMMUNICATION
Zhenhai Wen et al.
An electrochemically neutralized energy-assisted low-cost acid-alkaline electrolyzer for energy-saving electrolysis hydrogen generation

This is an Accepted Manuscript, which has been through the Royal Society of Chemistry peer review process and has been accepted for publication.

Accepted Manuscripts are published online shortly after acceptance, before technical editing, formatting and proof reading. Using this free service, authors can make their results available to the community, in citable form, before we publish the edited article. We will replace this Accepted Manuscript with the edited and formatted Advance Article as soon as it is available.

You can find more information about Accepted Manuscripts in the Information for Authors.

Please note that technical editing may introduce minor changes to the text and/or graphics, which may alter content. The journal's standard Terms & Conditions and the Ethical guidelines still apply. In no event shall the Royal Society of Chemistry be held responsible for any errors or omissions in this Accepted Manuscript or any consequences arising from the use of any information it contains.

ROYAL SOCIETY OF CHEMISTRY

rsc.li/materials-a

Confined-space synthesis of Zr-, Ti-, and Ti-Zr-oxocluster-based hybrid nanoparticles as catalysts for H_2O_2-mediated oxidations

Davide Vendrame[1], Giulia Bragaggia[1,2], Alessandro Dolmella[1,3], Giacomo Saielli[1,4], Mauro Carraro[1,4]*, Silvia Gross[1,2,5]*

[1] Università degli Studi di Padova, Dipartimento di Scienze Chimiche, via Marzolo 1, 35131, Padova, Italy

[2] INSTM, Consorzio Interuniversitario per la Scienza e Tecnologia dei Materiali, Via Giusti 9, 50121 Firenze, Italy

[3] Università degli Studi di Padova, Dipartimento di Scienze del Farmaco, via Marzolo 5, 35131, Padova, Italy

[4] CNR, Istituto per la Tecnologia delle Membrane, Sede Secondaria di Padova, via Marzolo 1, 35131, Padova, Italy

[5] Karlsruher Institut für Technologie (KIT), Institut für Technische Chemie und Polymerchemie (ITCP), 76131 Karlsruhe, Germany

Abstract

Hybrid organic–inorganic nanoparticles were synthesized by incorporating covalently embedded monometallic (Ti or Zr) and bimetallic (Ti–Zr) oxoclusters, functionalized with polymerizable methacrylate ligands, into a polymethylmethacrylate (PMMA) matrix. Nanoparticles were synthesized via photoactivated free-radical copolymerization within direct (oil-in-water) miniemulsion droplets, serving as confined nanoreactors. This synthetic approach yielded spherical hybrid nanoparticles with an average diameter of 76 ± 50 nm. Considering the ability of d^0 early transition metals to coordinate and activate the H_2O_2 molecule, the catalytic activity of these materials was investigated in heterogeneous oxidation reactions. Their catalytic performance was initially evaluated in the oxidation of methyl p-tolyl sulfide, representing the first example of Ti- and Ti–Zr-oxocluster-based hybrid materials as catalysts in a peroxidation reaction. Among them, the monometallic Ti-based materials demonstrated superior conversion, selectivity, and reaction rate. Subsequently, the catalysts were tested for the oxidation of benzyl alcohol and for the epoxidation of cyclooctene, demonstrating the potential application of oxocluster-based catalysts for primary alcohol and alkene oxidations. Notably, the hybrid based on $Ti_4O_2(^iOPr)_6(OMc)_6$ displayed the highest conversions and reaction rate also for such reactions. These findings highlight the potential application of miniemulsion-synthesized oxocluster-based hybrid nanoparticles as heterogeneous catalysts for the oxidation of various organic substrates. Moreover, preliminary hypotheses regarding the formation of the active peroxometal species were formulated, based on density functional theory (DFT) calculations.

Introduction

The broad plethora of possible combinations of functional organic molecules and inorganic building blocks is one of the main driving forces for the exploration of novel multifunctional organic-inorganic hybrid materials. These compounds, mostly consisting of an inorganic core embedded in an organic matrix, display a great variability, in terms of chemical nature and structure of the components, leading to a fine-tuning of the material properties.[1,2] In particular, great interest is addressed to class II hybrids, which are distinguished from class I hybrids by the covalent linkage between the building block, where the inorganic domain is embedded into a polymeric matrix through a copolymerization with suitable organic monomers. The strong interactions between the two components allows for a better distribution of the inorganic filler in the polymeric matrix, while minimizing phenomena like phase separation, migration, aggregation, and leaching.[3,4] In the last two decades, several types of inorganic building blocks have been employed to synthesize hybrid materials, such as polyhedral oligomeric silsesquioxanes (POSS)[5,6], polyoxometalates (POM)[7–9] or oxoclusters of early transition metals.[3,10–12]

Transition metal oxoclusters, with the general formula $M_xO_y(OH)_w(OC(O)R)_z$, are formed by a polyhedral inorganic core composed of M-O-M bridges (where M is typically an early transition metal

in its highest oxidation state) coordinated by bidentate organic ligands, typically carboxylates. The functionalization of the inorganic core with ligands containing polymerizable moieties, such as C=C bonds, makes these compounds suitable building blocks for the synthesis of cross-linked hybrid materials with an appropriate organic comonomer.[3,10,12,14,15]

The incorporation of early transition metal oxoclusters has been proven to enhance the mechanical and thermal resistance of the resulting polymeric material;[3,10,12,16–18] moreover, the final materials swell in organic solvent,[19] enabling their application as a heterogeneous catalysts with tunable substrate access to the catalytically active center.[17,20] Compounds based on early transition metals in their highest oxidation state (d^0) display interesting catalytic properties, in particular towards the activation of hydrogen peroxide, for the oxidation of different substrates, such as olefins, sulfides, sulfoxides, and alcohols.[18,21–27] Faccioli et al. described the catalytic activity of zirconium-based oxoclusters for the homogeneous catalytic oxidation of sulfur-based substrates in the presence of hydrogen peroxide.[27] Although the catalysts showed low oxidative and hydrolytic stability in the reaction environment, their incorporation in a polymethyl methacrylate (PMMA) matrix allowed to pursue a higher overall stability of the resulting heterogeneous catalysts, thus increasing their catalytic performance, while enabling their recovery and recycle.[18,20] More recently, Benedetti et al. described the successful incorporation of the oxocluster $Zr_4O_2(OMc)_{12}$ (OMc = methacrylate) (in the following labelled as **Zr₄**) in a PMMA matrix through a polymerization process carried out in the confined space of direct (oil-in-water) miniemulsion droplets.[28] The miniemulsion polymerization allowed to obtain a final hybrid material in the form of nanoparticles featuring high specific surface area, enhanced dispersibility, with tunable behaviour in terms of dimensions, cross-linking degree, and swelling.[29–33]

While it is known that Zr-oxocluster-based hybrids are effective catalysts for the oxidation of organic sulfide in the presence of H_2O_2,[18,20,27,28,34] it should be emphasized that Ti(IV) compounds are generally more efficient for H_2O_2 activation, encompassing a range of structures from mononuclear[35] and dinuclear complexes[36] to polyoxometalates.[37] This suggests that hybrid materials incorporating Ti- or bimetallic Ti-Zr oxoclusters could offer superior catalytic activity for sulfide oxidation compared to their Zr analogues. Considering the advantages of nanoparticle synthesis via miniemulsion, we hypothesized that Ti- and Ti-Zr oxocluster-based hybrid nanoparticles could represent a significant advancement in heterogeneous catalysts for sulfide oxidation mediated by H_2O_2.

Herein, we report, to the best of our knowledge, for the first time the synthesis and characterization of hybrid organic-inorganic nanoparticles based on monometallic (Ti) and bimetallic (Ti-Zr) oxoclusters covalently embedded within a PMMA matrix. These nanoparticles were prepared using a photoactivated free-radical copolymerization conducted in direct miniemulsion droplets. Their catalytic activity was systematically evaluated in the oxidation of methyl p-tolyl sulfide using H_2O_2 as the oxidant. Furthermore, the catalytic performance was explored with respect to the oxidation of benzyl alcohol and cyclooctene, highlighting the potential application of oxocluster-based catalysts for the oxidation an alcohols and alkenes. DFT calculations were also performed to demonstrate the formation of peroxo species via ligand exchange with H_2O_2.

Experimental Section

Materials

Zirconium n-butoxide (Zr(^{n}OBu)$_4$, Merck, 80% wt. in n-butanol), zirconium n-propoxide (Zr(^{n}OPr)$_4$, Merck, 70% wt. in n-propanol), titanium isopropoxide (Ti(^{i}OPr)$_4$, Merck, 97% wt. in isopropanol), titanium n-butoxide (Ti(^{n}OBu)$_4$, Merck, 98% wt. in n-butanol) and methacrylic acid (Merck, 99% wt. stabilized, filtered through alumina to remove the polymerization inhibitor) were employed for the synthesis of the oxoclusters. Methyl methacrylate (MMA, Merck, 98% wt. stabilized) was employed as the comonomer for the synthesis of the hybrids, after filtration through alumina to remove the polymerization inhibitor. Sodium n-dodecyl sulphate (SDS, 99% wt., Alfa Aesar), hexadecane (99%

wt., Alfa Aesar), and Irgacure 2959 (BASF) were employed in the synthesis of the hybrid nanoparticles. Hydrogen peroxide (Merck, 35% wt. in water), methyl *p*-tolyl sulphide (Merck, 99% wt.), benzyl alcohol (Merck, 99% wt.), cyclooctene (Merck, 95% wt.), and acetonitrile (Merck, ≥99% wt.) were employed in the catalytic tests. Dichloromethane (Merck, ≥99.9% wt.), *n*-undecane (Merck, ≥99% wt.), and polystyrene-supported triphenylphosphine (Merck) were employed for the preparation of the GC analysis samples.

Synthesis of the oxoclusters

Synthesis of $Zr_4O_2(OMc)_{12}$ (**Zr$_4$**)

The **Zr$_4$** oxocluster was synthesized according to a previously reported procedure by the reaction of zirconium *n*-butoxide with methacrylic acid in a 1:7 molar ratio.[19]

6.619 of an 80% solution of zirconium *n*-butoxide were added to 8.401 g of methacrylic acid under Ar using a standard Schlenk line setup. After mixing at room temperature, the solution was allowed to stand for 2 days. The colourless crystals formed were decanted and dried under vacuum for 4h (80% yield). The crystalline structure of the oxocluster, previously reported in the literature,[19] was confirmed by measuring the unit cell dimensions with a single-crystal X-ray diffraction technique (Table S1) and through FT-IR ATR and Raman spectroscopy (Figure S3).

Synthesis of $Ti_4O_2(^iOPr)_6(OMc)_6$ (**Ti$_4$**) and $Ti_6O_4(^nOBu)_8(OMc)_8$ (**Ti$_6$**)

The **Ti$_4$** and **Ti$_6$** oxoclusters were synthesized according to previously reported procedures by the reaction of titanium isopropoxide, in the case of **Ti$_4$**, or titanium *n*-butoxide, in the case of **Ti$_6$**, with methacrylic acid in a 1:2.2 molar ratio.[38]

For the synthesis of **Ti$_4$**, 4.012 g of a 97% solution of titanium isopropoxide were added to 2.347 g of methacrylic acid. For the synthesis of **Ti$_6$**, 4.998 g of a 98% solution of titanium *n*-butoxide were added to 2.720 g of methacrylic acid. After mixing at room temperature and under Ar atmosphere, using a standard Schlenk line setup, the solution was allowed to stand for one month. The yellowish crystals formed were decanted and dried under vacuum for 4h (50% yield for **Ti$_4$**, 67% yield for **Ti$_6$**). The crystalline structures of the oxoclusters, previously reported in the literature,[38] were confirmed by measuring the unit cell dimensions with a single-crystal X-ray diffraction technique (Table S1) and through FT-IR ATR and Raman spectroscopy (Figure S4 and S5).

Synthesis of $Ti_2Zr_4O_4(^nOBu)_2(OMc)_{14}$ (**Ti$_2$Zr$_4$**) and $Ti_4Zr_2O_4(^nOBu)_6(OMc)_{10}$ (**Ti$_4$Zr$_2$**)

The **Ti$_2$Zr$_4$** and **Ti$_4$Zr$_2$** oxoclusters were synthesized according to a reported procedure.[39] The **Ti$_2$Zr$_4$** oxocluster was synthesized by reaction of titanium *n*-butoxide, zirconium *n*-butoxide and methacrylic acid in a 1:2:12.6 molar ratio. The **Ti$_4$Zr$_2$** oxocluster was synthesized by reaction of titanium *n*-butoxide, zirconium *n*-propoxide and methacrylic acid in a 1:1:8.4 molar ratio.

For the synthesis of **Ti$_2$Zr$_4$**, 2.652 g of a 98% solution of titanium *n*-butoxide, 7.246 g of a 80% solution of zirconium *n*-butoxide were added to 8.341 g of methacrylic acid. For the synthesis of **Ti$_4$Zr$_2$**, 2.334 g of of a 98% solution of titanium *n*-butoxide, 3.218 g of a 80% solution of zirconium *n*-butoxide were added to 4.987 g of methacrylic acid. After mixing at room temperature and under argon atmosphere, using a standard Schlenk line setup, the solution was allowed to stand for one month. The yellowish crystals formed were decanted and dried under vacuum for 4h (67% yield for **Ti$_2$Zr$_4$**, 85% yield for **Ti$_4$Zr$_2$**). The crystalline structures of the oxoclusters, previously reported in the literature,[39] were confirmed by measuring the unit cell dimensions with a single-crystal X-ray diffraction technique (Table S1) and through FT-IR ATR and Raman spectroscopy (Figure S6 and S7).

Synthesis of the hybrid materials

Hybrid materials in the form of nanoparticles were obtained through a free-radical polymerization, between the oxocluster and MMA, conducted within the confined space of direct (oil-in-water)

miniemulsion droplets. The hydrophobic phase, consisting of one of the oxoclusters and MMA in a 1:100 molar ratio, hexadecane (4.2% wt. of the total mass of the monomers) as a hydrophobic agent, and Irgacure 2959 (3% wt. of the total mass of the monomers) as polymerization initiator, was stirred at 1500 rpm for 15 min to dissolve the oxocluster crystals. The hydrophilic phase consisted of an aqueous solution of SDS 3 g/L. The weight ratio between the hydrophobic and the hydrophilic phase was set equal to 1:4.[28] The two phases were pre-emulsified by stirring at 1500 rpm for 15 minutes and then homogenized by ultrasonication (3 min, 70% intensity, 644 W, Laborsonic P Sartorius Stedim Sonicator) while cooling the solution with an ice−water bath. The polymerization was activated by UV radiation (Hg-vapor UV lamp operating at 400 W) placing the miniemulsion under the lamp (constant stirring during the polymerization), and different polymerization times were tested. The obtained hybrids were isolated and washed through three steps of centrifugation (the first two steps with water, the last one with acetonitrile; 15000 rpm for 10 minutes) and then dried under vacuum for 12 hours.

Characterization methods

The hybrid materials were characterized by FT-IR in an Attenuated Total Reflectance (ATR) mode (diamond crystal) using a Thermo NEXUS 870 FT-IR NICOLET instrument. The wavelength range was 4500-500 cm^{-1} recording 64 scans with a resolution of 4 cm^{-1}.

Raman spectra were collected by using a Thermo DXR Raman Microscope equipped with a 532 nm laser as excitation source operating at 10 mW power. The recorded range was 120-3500 cm^{-1} recording 64 scans for each sample with an exposure time of 1 s.

Low-angle XRD date were recorded using a Bruker AXS D8 Advance Plus diffractometer, equipped with a Cu Kα1,2 anode (λ = 1.5106 Å) and a LYNEXEYE XE-T detector in 1D mode. X-rays were generated by supplying a voltage of 40 kV and a current of 40 mA. The measurements were performed using the Bragg–Brentano geometry. The diffractograms were collected over the 0.4 – 10.0° 2θ range, with a step size of 0.02° 2θ and a nominal time per step of 1 s. A variable primary divergence slit opening (keeping the length of the illuminated specimen area constant to 25 mm) and a fixed secondary divergence slit opening (2.34°) were employed together with Soller slits with an aperture of 2.5°. A position-sensitive detector (PSD) opening of 0.4° was employed. Automatic air scatter knife positioning was used.

Thermogravimetric Analyses (TGA) were carried out to evaluate the inorganic content of the hybrid materials. The data were collected with a TGA Q500 TA Instruments with a ramp of 10 °C/min from 60 °C up to 800 °C under air flow.

Scanning electron microscopy (SEM) analysis was performed by using a Zeiss SUPRA 40VP instrument equipped with a detector Oxford INCA xsight X-ray. The accelerating potential was set at 5 kV.

Single Crystal X-Ray Diffraction analyses were collected on a Rigaku-Oxford Xcalibur Gemini EOS diffractometer, equipped with a 2K × 2K CCD area detector and sealed-tube Enhance (Mo) and (Cu) X-ray sources. The raw diffraction data were collected by means of ω-scan techniques at room temperature using graphite-monochromated Mo-K_α (λ = 0.71073 Å) or Cu-K_α (λ = 1.54184 Å) radiation in a 1024 × 1024 pixel mode and 2 × 2 pixel binning or (when necessary) 4 × 4 binning. Accurate unit cell parameters needed for comparison with reported known structures were obtained by the least-squares refinement of 21166/15900 ($Ti_2Zr_4O_4(O^nBu)_2(OMc)_{14}$), 4997/7267 ($Ti_4Zr_2O_4(O^nBu)_6(OMc)_{10}$), 5987/6703 ($Zr_4O_2(OMc)_{12}$), 10128/5816 ($Ti_4O_2(O^iPr)_6(OMc)_6$) and 6858/7169 ($Ti_6O_4(O^nBu)_8(OMc)_8$) strongest reflections chosen throughout the whole data collection. Data collection, reduction, and finalization were performed using the *CrysAlisPro* software, Versions 1.171.42.49 (Rigaku OD, 2022). Raw data were corrected for Lorentz / polarization effects. An empirical absorption correction was also performed by means of a multi-scan approach, with the scaling algorithm *SCALE3 ABSPACK*, using equivalent reflections.

The swelling experiments were carried out by immersing a weighted amount of hybrid material in acetonitrile for 72 h; after withdrawal from the solvent, the wet sample was weighted again. For the swelling test, the materials were synthesized with a photoactivated bulk polymerization. The swelling index (I_{sw}) was determined by the following formula:

$$I_{sw} = \frac{(wt_{wet} - wt_{dry})}{wt_{dry}} \text{ x } 100 \quad (1)$$

Computational details

DFT Calculations were performed using the software package Gaussian 16.[40] Based on the benchmark results reported in Ref.[41] concerning zirconium oxoclusters, we selected the PBE0 [42–44] functional and a basis set of triple-ζ quality, namely the 6-311g(d,p) for the light atoms and the LANL2TZ with effective core potentials for Zr and Ti; this was obtained from the Basis Set Exchange database.[45] Long-range solvent effects (acetonitrile) were included in the calculations using the PCM (Polarizable Continuum Model) model [46,47] as implemented in Gaussian 16. Starting geometries were obtained from the X-ray structures of the zirconium[19] [**Zr₄**] (CCDC deposition nr. 137083) and titanium[38] [**Ti₄**] (CCDC deposition nr. 167594) oxoclusters, respectively. All structures were first minimized in the gas phase and checked to be true minima by calculating the vibrational frequencies: no imaginary frequencies were found. Cartesian coordinates of the relevant systems can be found in the Computational Details in the Supporting Information.

Catalytic tests

In a typical oxidation reaction, a suitable quantity of hybrid nanoparticles, to provide 0.028 mmol of the embedded oxocluster, was added to 2.4 mL of acetonitrile, with 1 mmol of substrate (methyl p-tolyl sulphide, benzyl alcohol, or cyclooctene), in a small closed vial. Subsequently, 2 mmol of H_2O_2 (from a 35% wt aqueous solution) were added to the solution. The oxidation reaction was run at fixed temperature (50 °C) under stirring. Samples (50 μL) were withdrawn at selected time intervals and diluted in 1100 μL with a 10 mM solution of n-undecane (standard) in CH_2Cl_2 and treated with triphenylphosphine (supported on a poly(styrene/divinylbenzene) resin) as quencher for the residual oxidant. GC analyses were performed with a Shimadzu GC2010 equipped with an ionization flame detector and an Equity-5 (15 m × 0.1 mm) capillary column of poly(5%-diphenyl / 95%-dimethylsiloxane) with 0.1 mm film thickness ($T_{injection}$ = 270 °C; $T_{detection}$ = 280 °C; carrier gas: He; $T_{initial}$ = 90°C × 1 min; rate = 90 °C/min; T_{final} = 260 °C × 5 min). Retention times: n-undecane: 2.75 min; methyl p-tolyl sulfide: 3.23 min; methyl p-tolyl sulfoxide: 4.30 min; methyl p-tolyl sulfone: 4.55 min; cyclooctene: 1.59 min; cyclooctene oxide: 2.26 min; benzyl alcohol: 2.49 min; benzaldehyde: 2.11 min. Concentrations (C) of reactants and oxidation products were calculated by integration of chromatographic peaks (A) of the standard (S) and of the analytes (X), using the following calculated response factors $F = (A_S/C_S)/(A_X/C_X)$: F(undecane) = 1, F(methyl p-tolyl sulfide) = 0.66, F(methyl p-tolyl sulfoxide) = 0.64, F(methyl p-tolyl sulfone) = 0.64, F(cyclooctene) = 0.73, F(cyclooctene oxide) = 0.54, F(benzyl alcohol) = 0.51, F(benzaldehyde) = 0.53. Second order kinetic constants were determined performing a fitting on the experimental values with Scientist Micromath software. The results of the GC analyses are reported in Table S2 – S19.

Results and Discussion

Synthesis of Hybrid Nanoparticles

Following known procedures, five different oxoclusters were synthesized: $Zr_4O_2(OMc)_{12}$ [**Zr₄**],[19] $Ti_4O_2(O^iPr)_6(OMc)_6$ [**Ti₄**],[38] $Ti_6O_4(O^nBu)_8(OMc)_8$ [**Ti₆**],[38] $Ti_2Zr_4O_4(O^nBu)_2(OMc)_{14}$ [**Ti₂Zr₄**],[39] and $Ti_4Zr_2O_4(O^nBu)_6(OMc)_{10}$ [**Ti₄Zr₂**].[39] The structure of each synthesized oxocluster was confirmed through single-crystal XRD analysis. Table S1 reports the crystal cell parameters for all the oxoclusters and a match percentage to the structures already deposited in the CCDC.[48] For **Zr₄** the match points to the isostructural and isomorphous hafnium derivative, while for compound **Ti₆** the

known compound, with identical structure of the oxocluster moiety, is the *n*-propoxy analogue (in all cases the expected inorganic oxometallate core was unambiguously identified. A representative example of one of the structures, compared with the existing one (**Ti$_4$Zr$_2$**), is provided in the supporting information (Figure S1), where we also added a comparison of the experimental structure of **Ti$_6$** with the structure deposited in the CCDC (Figure S2). Moreover, the successful synthesis of the oxoclusters was also confirmed by FT-IR ATR and Raman spectroscopy. The FT-IR and Raman spectra of the oxoclusters are reported in Figures S3 – S7, along with the proposed interpretation based on IR and Raman spectra of Zr oxoclusters.[49]
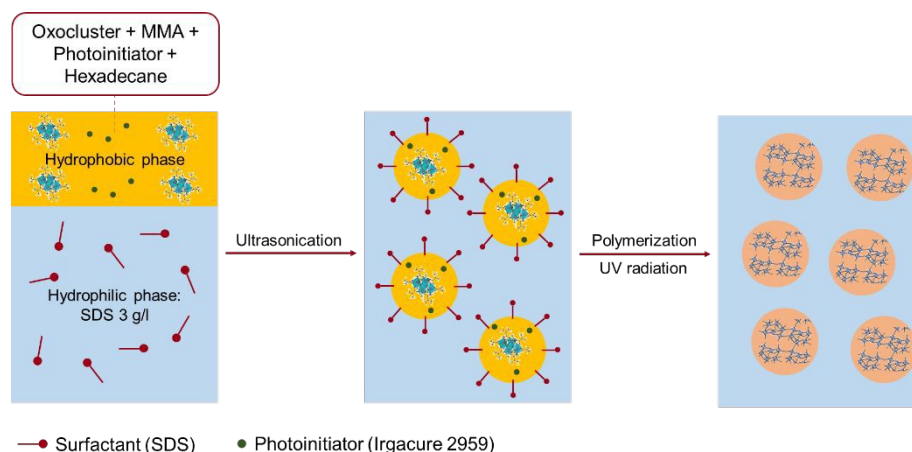

Figure 1. Schematic representation of the miniemulsion polymerization process carried out to obtain oxocluster-based hybrid nanoparticles.

Subsequently, the photoactivated free radical polymerization with methyl methacrylate (MMA) was carried out within direct (oil-in-water, o/w) miniemulsion droplets, as schematically reported in Figure 1. Sodium dodecyl sulfate (SDS) was chosen as the surfactant for the preparation of the miniemulsion, given the excellent results in terms of cross-linking and size distribution of the nanoparticles (NPs) reported in the work of Benedetti et al.[28] The latter also highlights the optimal hydrophobic (oxocluster + MMA) / hydrophilic (SDS aqueous solution 3 g/L) phase weight ratio of 1:4, in terms of miniemulsion stability (up to 72 hours) and NPs morphology. The oxocluster/MMA molar ratio was fixed at 1:100 for all the syntheses, since a previous study referred to this value as optimal for gaining a high swelling degree in organic solvents which, in turn, is related to the access of the substrates to catalytic active sites.[18,20] Various polymerization times were tested to obtain high values of polymerization degree (5 –50 min). In Table 1, all synthesized hybrid samples are reported. In Figure S8 – S12 the FT-IR ATR and Raman spectra of the hybrid materials are reported.

Table 1. List of synthesized oxocluster-based hybrid materials. Photoactivated free radical polymerization between the oxoclusters and MMA was carried out with reaction times ranging from 5 min to 50 min.

Sample	Oxocluster	Polymerization time (min)
Zr$_4$-5		5
Zr$_4$-10		10
Zr$_4$-20	Zr$_4$	20
Zr$_4$-30		30
Zr$_4$-40		40
Zr$_4$-50		50
Ti$_4$-20	Ti$_4$	
Ti$_6$-20	Ti$_6$	
Ti$_2$Zr$_4$-20	Ti$_2$Zr$_4$	20
Ti$_4$Zr$_2$-20	Ti$_4$Zr$_2$	

In order to evaluate the degree of polymerization of these hybrids, the **Zr$_4$**-based materials were characterized through infrared spectroscopy (ATR-FTIR) by comparing the areas of the signal

related to the C=C bond (1642 cm^{-1}) with the one of the C=O bond (1720 cm^{-1}).[50] **Zr$_4$**-based hybrids were selected as a benchmark to optimize the reaction time. The C=C/C=O area ratio can be correlated with the degree of polymerization of the material: the C=C bonds react during the free radical polymerization and their signal intensity decrease, whereas the C=O signal is taken as a reference as it remains unvaried, therefore their ratio should decrease as the polymerization proceeds.[50] In Table 2, the C=C/C=O ratios of the **Zr$_4$** oxocluster-based hybrid nanoparticles are reported. A comparison of the FTIR spectra of the samples **Zr$_4$**-5 and **Zr$_4$**-20 is reported in Figure S13.

Table 2. Degree of polymerization (evaluated from the area ratio of C=C / C=O IR signals) of the samples based on **Zr$_4$**.

Sample	Polymerization time (min)	Area C=C	Area C=O	Ratio (C=C/C=O) %
Zr$_4$-5	5	0.15	0.63	24
Zr$_4$-10	10	0.11	0.98	11
Zr$_4$-20	20	0.07	0.99	7
Zr$_4$-30	30	0.07	0.97	7
Zr$_4$-40	40	0.06	0.68	8
Zr$_4$-50	50	0.07	0.89	8

It is worth noting that as the polymerization time increases, from 5 min to 20 min, an increase of the degree of polymerization degree is observed. With polymerization times longer than 20 min, the polymerization extent does not change significantly; consequently, all the samples prepared with the other four oxoclusters underwent a 20 min long polymerization.

Due to the amorphous nature of the hybrid materials, XRD studies cannot provide detailed structural information. However, in Figure S14 of SI we show the diffractogram of a selected sample, **Zr$_4$**-20. The most notable feature is a very broad and low-intensity halo centred approximately at $2\theta = 5°$ and corresponding to a distance of ca. 18 Å. This feature might be related to the average separation between the clusters dispersed within the amorphous polymethacrylate matrix.

To evaluate the morphology of the nanoparticles and their size distribution, SEM measurements were carried out (Figure S15 – S19). As an example, in Figure 2 a SEM image of the sample **Zr$_4$**-20 is reported, along with a graphical representation of the size-distribution of the NPs. The spherical NPs display a broad size distribution with an average diameter of 76 nm (standard deviation = ± 50 nm).
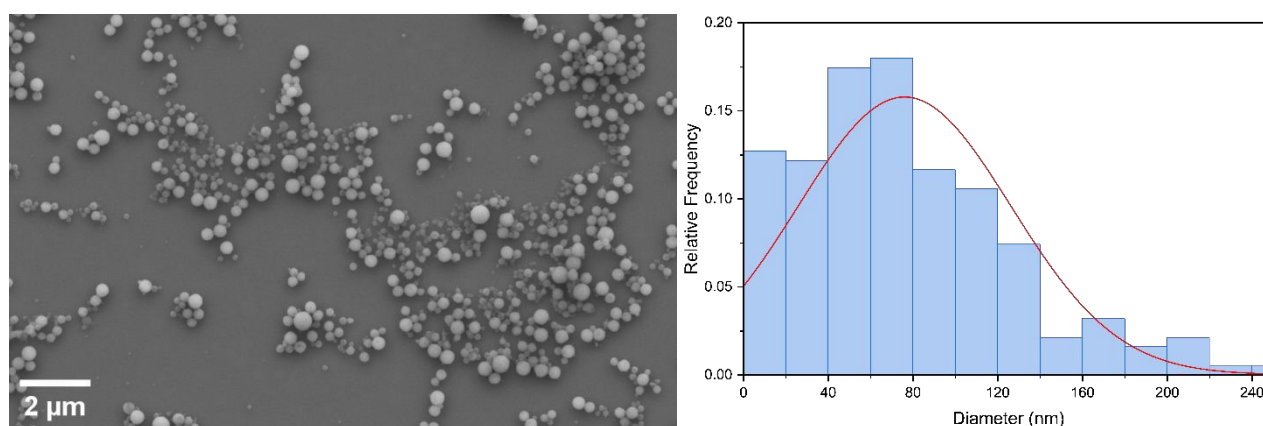

Figure 2. SEM image of the sample Zr$_4$-20 (on the left) and average size-distribution (on the right).

Since the concentration of the oxocluster in the polymer matrix determines the catalytic performances of the whole material, thermogravimetric analyses (TGA) were employed to evaluate the actual content of the oxocluster in the hybrid materials. The thermal decomposition in air of the oxoclusters produces a specific number of moles of TiO$_2$ and/or ZrO$_2$, depending on the chemical composition of the inorganic core; hence, by the quantification of the inorganic residue, it is possible
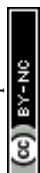
to estimate the real content of oxocluster embedded in the PMMA matrix. From the TGA results (Figure S20), it is possible to observe a first significant weight loss in the range of 60 – 290 °C, which was attributed to the removal of residual unreacted monomer and adsorbed species. In the range 290 – 450 °C the most intense weight loss was observed, which was ascribed to the degradation of the polymer matrix of the samples. A final weight loss, in the range 450 – 550 °C, was related to the degradation of the organic fraction of the oxocluster. The improved thermal stability of the hybrids confirmed the successful covalent incorporation of the oxoclusters, as can be highlighted by comparing the traces of the samples with that of pure PMMA (Figure S20, black line), which starts to decompose at a lower temperature, around 225 °C.[18–20] In Table 3 it is possible to observe how the detected residual weights (% wt.) for all the five hybrid materials are comparable with the theoretical ones. For the samples based on Ti_6, Ti_2Zr_4 and Ti_4Zr_2, the experimental inorganic residue is slightly higher than the expected value, probably due to a partial evaporation of the MMA during the polymerization process, owing to the heat generated by the UV lamp (~ 50°C). Moreover, some unreacted monomers were likely washed away during the recovery process.

Table 3. TGA weight percentages residues, based on the molar ratio between the oxocluster and monomer, of the most representative synthesized hybrid materials.

Sample	Theoretical Residue (% wt.)	Experimental Residue (% wt.)
Zr_4-20	4.3	3.9
Ti_4-20	2.9	2.9
Ti_6-20	4.0	5.0
Ti_2Zr_4-20	5.5	6.1
Ti_4Zr_2-20	6.2	7.5

Since the Zr and Ti ions are the active catalytic sites, the reaction solvent plays a fundamental role in enabling the diffusion of the reaction substrates and intermediates through the PMMA up to the oxoclusters core. To verify the accessibility to the metallic sites, swelling tests were performed with the solvent used for the catalytic tests, acetonitrile (ACN). The oxoclusters, being functionalized with several polymerizable groups, behave as cross-linking sites during the polymerization process, therefore, while the pure PMMA is soluble in many organic solvents (including ACN), the synthesized hybrid materials swell without solubilizing. Previous studies have already reported how the swelling degree is inversely proportional to the degree of cross-linking and, therefore, to the oxocluster concentration in the polymer matrix.[18,20] ACN, chosen as the reaction solvent, was confirmed to be the optimal choice for the oxidative desulfurization of methyl *p*-tolyl sulfide catalysed by Zr_4-based hybrids[18,20] likely due to its intermediate polarity ($E_T(30)$ = 46).[51] The obtained swelling degrees are reported in Table 4, while the mathematical equation used for its quantification is reported in the Experimental Section.

Table 4. Swelling degrees of the hybrid materials in ACN after 72 hours.

Sample	Zr_4-20	Ti_4-20	Ti_6-20	Ti_2Zr_4-20	Ti_4Zr_2-20
I_{sw} (%)	59	73	67	49	55

It is worth noting that the highest swelling values were obtained for hybrids based on Ti_4 and Ti_6. This result can be explained by considering that these two oxoclusters, containing 6 and 8 polymerizable functional groups (C=C), respectively, form materials with a lower degree of cross-linking than those obtained from oxoclusters with a higher number of C=C bonds (12 for Zr_4, 14 for Ti_2Zr_4 and 10 for Ti_4Zr_2).

Catalytic tests

Oxidation of Methyl p-tolyl Sulfide

It is well known from our previous works that peroxides coordinated to Zr-oxocluster display a high reactivity towards the oxidation of organic sulfides,[27] and the selectivity for the sulfones is further

enhanced by the presence of the polymeric matrix, owing to the increased affinity for the intermediate sulfoxide substrates.[18,20,28] The synthesized hybrid materials were tested as heterogeneous catalysts in the two-step oxidation of methyl p-tolyl sulfide (**S**) to the corresponding sulfoxide (**SO**) and sulfone (**SO$_2$**) in the presence of hydrogen peroxide (H$_2$O$_2$), as schematically reported in Figure 3
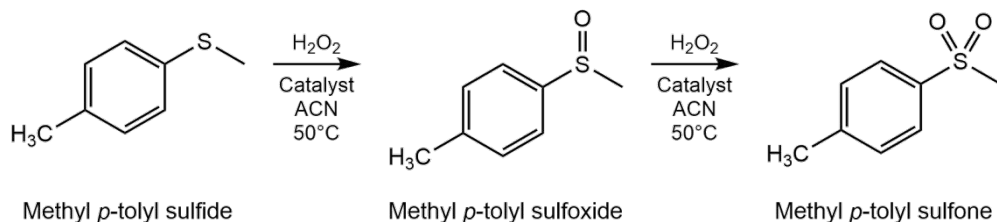
.

Figure 3. Scheme of the oxidation reaction of methyl p-tolyl sulfide (**S**) to the corresponding sulfoxide (**SO**) and sulfone (**SO$_2$**).

The percentage molar ratio between the oxocluster in the polymer matrix and **S**, was set to 0.28%; while the molar ratio between **S** and H$_2$O$_2$ was 1:2. The temperature was fixed at 50°C and the reaction was carried out for 24 hours. The conversion, initial rate (calculated in the first 5 minutes of the reaction) and the two kinetic constants k_1 and k_2 (first and second reaction step, respectively), are reported in Table 5. The full reaction profiles, obtained by monitoring the reaction through gas-chromatographic (GC) analyses (Table S2 – S19), are reported in the Supporting Information (Figure S21).

Table 5. Results of the catalytic tests of the oxidation of methyl p-tolyl sulfide (**S**) to methyl p-tolyl sulfoxide (**SO**) and methyl p-tolyl sulfone (**SO$_2$**) in terms of conversion, selectivity, initial rate (R_0, calculated in the first 5 minutes) and rate constants (k_1: first reaction step, k_2: second reaction step).

Catalyst	Conversion % 5 min	Conversion % 10 min	Conversion % 30 min	SO:SO$_2$ 5 min	SO:SO$_2$ 10 min	SO:SO$_2$ 30 min	R_0 mM/s	k_1, k_2 M^{-1}s^{-1}	$\frac{k_1}{k_2}$
No cat.	9	12	25	93:7	93:7	89:11	0.10	1.3×10^{-4} / 3.7×10^{-5}	3.5
Zr$_4$-20	77	86	95	24:76	16:84	9:91	1.03	1.7×10^{-2} / 9.5×10^{-3}	1.7
Ti$_4$-20	>99	>99	>99	5:95	4:96	4:96	1.33	1.2×10^{-1} / 9.2×10^{-2}	1.3
Ti$_6$-20	>99	>99	>99	5:95	5:95	3:97	1.31	1.2×10^{-1} / 9.0×10^{-2}	1.3
Ti$_2$Zr$_4$-20	96	96	97	29:71	29:71	28:72	1.27	8.8×10^{-2} / 4.8×10^{-2}	1.8
Ti$_4$Zr$_2$-20	95	95	96	41:59	41:59	40:60	1.26	7.9×10^{-2} / 3.4×10^{-2}	2.4
Ti$_4$	46	72	99	87:13	86:14	73:27	0.62	3.6×10^{-3} / 7.7×10^{-4}	4.6

Journal of Materials Chemistry A Accepted Manuscript

Reaction conditions: a suitable quantity of catalysts, to provide 0.028 mmol of the embedded oxocluster, was added to 2.4 mL of ACN, with 1 mmol of methyl p-tolyl in a small, closed vial. Subsequently, 2 mmol of H_2O_2 (from a 35% wt. aqueous solution) were added to the solution. The reaction was run at fixed temperature (50 °C) under stirring for 24 hours.

It should be noted that there was a significant improvement in the reaction rate, conversion of **S** and selectivity towards **SO_2** going from the uncatalyzed reaction (first row) to the reaction carried out in the presence of the hybrid materials. Almost quantitative values of conversion and selectivity towards **SO_2** were obtained with catalysts based on **Zr_4**, **Ti_4**, and **Ti_6**. Moreover, the catalysts **Ti_4**-20 and **Ti_6**-20 showed the highest initial rate ($R_0 > 1.3$ mM/s). Lower conversions and selectivity were, instead, obtained with the two bimetallic catalysts **Ti_2Zr_4**-20 and **Ti_4Zr_2**-20. Nevertheless, the initial rates were similar to those obtained with the Ti-based catalysts.

On one hand, the better catalytic performances of **Ti_4**-20 and **Ti_6**-20 can be justified by the higher swelling degree in the reaction solvent, which provides easier access to the catalytic active sites of the catalyst. Furthermore, the higher activity of Ti(IV) compounds for the H_2O_2 activation agrees with the results reported in previous studies, in which catalysts based on d^0 transition metals as Mo, W, V[24,52–54] and Ti,[55] were shown to have greater efficiency than Zr mononuclear compounds.[56] Ti^{4+}, in particular, has a smaller ionic radius and a greater electrophilicity Than Zr^{4+}, which likely contributes to its superior performance in H_2O_2 activation.

Comparing the catalytic performances of the sample **Zr_4**-20 with those of the same hybrid material obtained from a bulk thermal activated polymerization, reported in our previous work,[18] (Table 6) it is possible to observe that the nanosized catalyst (**Zr_4**-20) possesses better catalytic properties (Figure S21). In particular, as reported in Table 6, both the conversion of **S** and the selectivity towards **SO_2** are higher using the nanoparticles than the bulk-synthetized catalyst. Also, the initial rate R_0 is almost 10 times higher for the nanoparticles than the bulk.

Table 6. Comparison of the catalytic results for the oxidation of **S** with the catalyst **Zr_4**-20 and **Zr_4**-Bulk, the latter reported as $Zr_4MMA(1:100)$ in our previous work.[18] The reaction conditions were the same for both the tests.

Catalyst	Conversion % 1 h	Conversion % 4 h	SO:SO₂ 1 h	SO:SO₂ 4 h	R₀ mM/s
Zr_4-Bulk[18]	84	95	21:79	9:91	0.11
Zr_4-20	98	99	5:95	1:99	1.03

The superior catalytic activity of the nano-sized catalyst compared to its bulk-synthesized counterpart can be attributed to its greater specific surface area and higher density of accessible active sites. This effect is further enhanced by the miniemulsion technique, which creates a controlled, compartmentalized environment that improves the distribution and accessibility of active sites, unlike the less controlled conditions of bulk synthesis. Based on these results, it has been demonstrated that the miniemulsion technique provides nanoparticles with excellent catalytic properties for the oxidation of **S** and, for **Zr_4**-20, higher than those obtained with the **Zr_4**-based bulk-synthetized material.

To assess the role of the PMMA matrix on the catalytic properties of the hybrid material, the pure **Ti_4** oxocluster was tested as catalyst for the oxidation of **S** without varying the reagents/oxocluster ratio. As it is possible to observe in Table 5, last row, **S** is almost quantitatively oxidized after 30 min, as for **Ti_4**-20 and **Ti_6**-20, but the R_0 value (0.62 mM/s) is less than half of that for **Ti_4**-20 (1.33 mM/s). Furthermore, the selectivity towards **SO_2** is clearly lower with the free oxocluster, as reflected by the higher ratio k_1/k_2, and an almost quantitative conversion to the most oxidized product, 3:97 (**SO:SO₂**) is reached only after 8 hours (Figure S24). In light of this result, it is possible to confirm that embedding the oxoclusters in the PMMA matrix enables their stabilization in the reaction environment and increases the overall catalytic activity of the resulting hybrid material.[18,20,28]

As pointed out in a recent study,[57] the mechanism involved in the metal-catalyzed sulfoxidation reaction is quite variable and depends on many factors, such as coordination geometry, steric hindrance and ionic radius of the metal centre. In the case of oxocluster-based catalysts, the intimate catalytic mechanism is still unknown and theoretical mechanistic studies are needed to understand the catalytic behaviour of these compounds. In order to shed some light on the different catalytic activity of the Ti-based and Zr-based materials, we carried out some preliminary DFT calculations of the reaction between Ti_4 or Zr_4 oxocluster and H_2O_2 involving the exchange of one ligand "A" with the hydroperoxide anion:

$$M_4A + H_2O_2 \rightarrow M_4OOH + HA \tag{2}$$

where A is either methacrylate (MA) or ^iPrO and M_4 is either Ti_4 or Zr_4. The adduct of HOO^- with the metal center is, in fact, considered to be the first relevant intermediate in similar reaction mechanisms involving both discrete structures[22] and oxide surfaces.[58] The results of the calculations are reported in Table 7. For each oxocluster, we considered four possible positions where a ligand could be replaced by the hydroperoxide anion. Concerning Ti_4, these are the three non-equivalent positions involving the bridging MA anions (labeled MA-n, n=1, 2, 3 in Table 7, see also Figures S25-S29 in Supporting Information) and one position of the ^iPrO ligand. On the other hand, for Zr_4 only the four non-equivalent positions (bridging or chelating) of MA (labelled MA-n, n=1, 2, 3, 4 in Table 7, see the corresponding Figures S30-S34 in Supporting Information) were considered, due to the lack of alkoxy ligands. The cartesian coordinates can be found in the Computational Details section of the Supporting Information.

Table 7. Calculated ΔE for the reactions of eq. 2 in kJ/mol. Level of theory PBE0(PCM)/triple- ζ.

Entry	Oxocluster	A[1]	ΔE (kJ/mol)
1	Ti_4	MA-1	15.3
2	Ti_4	MA-2	6.7
3	Ti_4	MA-3	39.0
4	Ti_4	iPrO	-5.1
5	Zr_4	MA-1	-5.6
6	Zr_4	MA-2	21.2
7	Zr_4	MA-3	-13.2
8	Zr_4	MA-4	16.9

[1]The numbering of the structures obtained for Ti_4 and Zr_4 has the only purpose of listing them and there is no correlation between the same MA-n of the two oxoclusters.

The results of the calculations suggest that the Zr_4 oxocluster forms a more stable complex with the hydroperoxide (entry 7 in Table 7, -13.2 kJ/mol) compared to the most stable complex found for Ti_4 (entry 4 in Table 7, -5.1 kJ/mol). While for Zr_4 the chelating MA-3 is the favourite position to replace, for Ti_4, the presence of a monodentate ligand as ^iPrO may favour the exchange. It is noteworthy that the Zr_4 MA-3 structure features a hydroperoxide anion coordinated to the Zr center by both oxygens, as represented in Figure S33 in the Supporting Information. Instead, in the Ti_4-^iPrO structure the HOO^- is bonded to the Ti centre by just one oxygen and the other OH group weakly H-bonded with a nearby ligand (Figure S28). These results are consistent with the typical coordination numbers of Ti and Zr, which are 6 and 8, respectively and with the smaller radius and higher electronegativity of Ti with respect to Zr.[59] The relatively higher instability of Ti_4-OOH complex could be thus correlated with its higher catalytic activity, as experimentally observed. Further studies, which are outside the scope of the present investigation, are necessary to fully elucidate the reaction mechanism and potential energy surface and will be reported in due time.

Benzyl alcohol and cyclooctene oxidation

Considering the good results obtained for the sulfide oxidation, the hybrid materials were also tested in the oxidation of benzyl alcohol (**BzOH**) and cyclooctene (**C**) using the same reaction conditions tested for the oxidation of **S** (including the molar ration between substrate and H_2O_2 equal to 1:2). We chose to explore the reactivity toward these compounds considering that the oxidation of primary

and secondary alcohols[24,60–62] and the epoxidation of olefins[63] are among the most important reactions in organic chemistry, since the obtained products (aldehydes, carbocyclic acids, or epoxides) are important intermediates in the synthesis of many fine chemicals and pharmaceuticals.[62,64]

The results are reported in Table 8, for the oxidation of **BzOH**, and in Table 9, for the oxidation of **C**. The reaction profiles of the benzyl alcohol and cyclooctene oxidations are reported in the Supporting Information (Figure S22 and S23, respectively).

Table 8. Results of the catalytic tests of the oxidation of benzyl alcohol (**BzOH**) to benzaldehyde (**BzO**) in terms of conversion, initial rate (R_0, calculated in the first 5 minutes), and second order rate constant.

Benzyl alcohol   Benzaldehyde
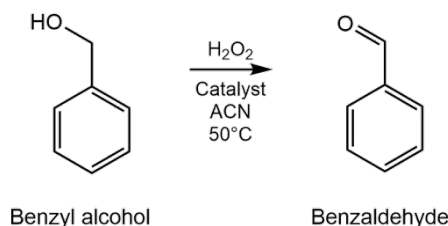
Catalyst	Conversion % 1 h	Conversion % 4 h	Conversion % 24 h	R_0 (µM/s)	k ($M^{-1}s^{-1}$)
No cat.	5	5	5	36	2.8×10^{-5}
Zr_4-20	6	8	11	52	6×10^{-5}
Ti_4-20	11	17	19	57	8×10^{-4}
Ti_6-20	8	10	13	50	9.3×10^{-4}
Ti_2Zr_4-20	5	8	11	51	3.2×10^{-4}
Ti_4Zr_2-20	6	8	10	48	4.3×10^{-4}

Reaction conditions: a suitable quantity of catalysts, to provide 0.028 mmol of the embedded oxocluster, was added to 2.4 mL of ACN, with 1 mmol of benzyl alcohol in a small, closed vial. Subsequently, 2 mmol of H_2O_2 (from a 35% wt aqueous solution) were added to the solution. The reaction was run at fixed temperature (50 °C) under stirring for 24 hours.

Table 9. Results of the catalytic tests of the oxidation of cyclooctene (**C**) to cyclooctene oxide (**CO**) in terms of conversion, initial rate (R_0, calculated in the first 5 minutes), and second order rate constant.

Cyclooctene   Cyclooctene oxide
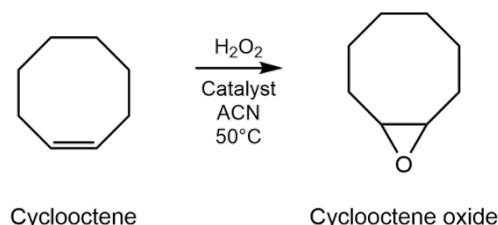
Catalyst	Conversion % 1 h	Conversion % 4 h	Conversion % 24 h	R_0 (µM/s)	k ($M^{-1}s^{-1}$)
No cat.	0	0	0	0	0
Zr_4-20	0	2	6	2	1.9×10^{-6}
Ti_4-20	21	31	40	46	1.2×10^{-4}
Ti_6-20	16	18	22	42	1.3×10^{-4}
Ti_2Zr_4-20	4	9	12	29	1.7×10^{-5}
Ti_4Zr_2-20	5	8	9	14	2.4×10^{-5}

Reaction conditions: a suitable quantity of catalysts, to provide 0.028 mmol of the embedded oxocluster, was added to 2.4 mL of ACN, with 1 mmol of cyclooctene in a small, closed vial. Subsequently, 2 mmol of H_2O_2 (from a 35% wt aqueous solution) were added to the solution. The reaction was run at fixed temperature (50 °C) under stirring for 24 hours.

For the oxidation of **BzOH**, no formation of benzoic acid was observed. A net increase of conversion and initial rate is observed in all the reactions carried out in the presence of hybrid nanoparticles compared to the uncatalyzed reaction (first row). The highest conversion of **BzOH** (19%, after 24 hours) and initial rate (57 µM/s) were obtained with **Ti_4**-20.

The oxidation of **C** to the corresponding epoxide **CO** does not take place in the absence of the catalyst, while the best performing catalyst was again **Ti_4**-20, with a conversion of 40% after 24 hours and an initial rate of 42 µM/s. As for the oxidation of **S**, on one side this result may be correlated to

the higher swelling degree of **Ti₄**-20 in acetonitrile, and hence to easier access to the catalytic active sites, and to the formation of a more reactive Ti-OOH complex.

Even if the conversion values obtained for **BzOH** and **C** oxidation are lower than those reported for some Ti- and Zr-polyoxometalates for alcohols and alkenes oxidations,[65–67] and will require a careful optimization in terms of conditions and of H_2O_2 amount/excess, these results underline the potential applications of oxocluster-based catalysts also for these kinds of reactions.

Catalysts Stability Evaluation

The results of our two previous studies,[18,20] in which **Zr₄**-based hybrids were tested as catalysts for the oxidation of organic sulfones, confirmed through XAS analyses that the oxoclusters crystal structure remains unchanged after the catalytic tests, indicating that the oxocluster within the PMMA matrix possesses the same structure as the pure **Zr₄** oxocluster. While we aimed to confirm the unaltered crystal structure of the oxoclusters after the catalytic tests, the amorphous nature of these hybrid materials prevents the use of XRD studies to directly investigate the crystal structure before and after the catalytic studies. Nevertheless, the retention of the oxocluster structure within the PMMA was evaluated using Raman spectroscopy.

At the end of the catalytic turnover (24 h), the reaction mixtures were centrifuged to separate the catalysts which were purified through two steps of centrifugation with water, and the last one with acetonitrile. Finally, the catalysts were placed under vacuum to remove the residual solvent.
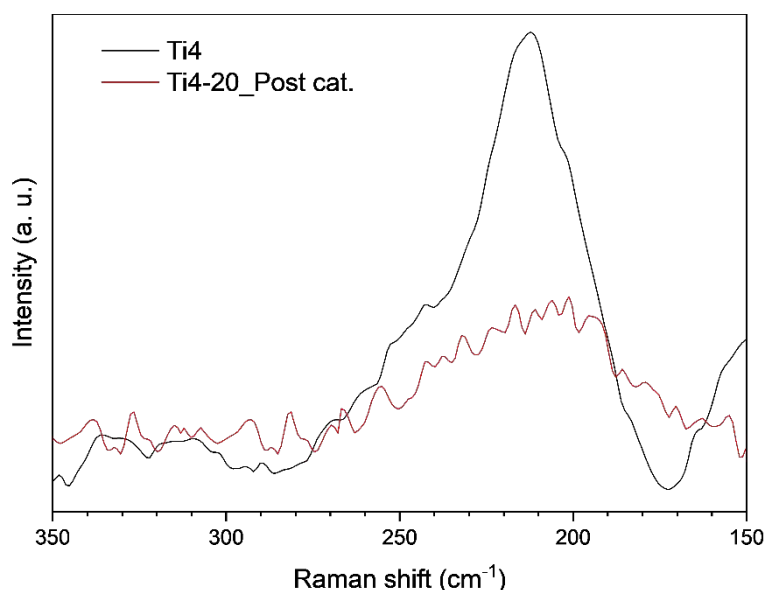

Figure 4. Comparison of the Raman spectra of **Ti₄** oxocluster (black line) and **Ti₄**-20 recovered after the catalysis (red line).

The signals associated with the vibrational modes of the M-O-M bond consist, typically, in two peaks present in the range 100-300 cm⁻¹.[27,68] In Figure 4, the Raman spectra of the oxocluster **Ti₄** and the correspondent hybrid **Ti₄**-20 recovered after the catalysis are reported (full-range spectra are reported in Figure S4 for **Ti₄** and S36 for **Ti₄**-20). While the signal of the Ti-O-Ti bond, centred at ~ 210 cm⁻¹ is easily detected for the pure oxocluster (black line), for the hybrid material the signals are less intense due to the dilution of the oxocluster in the hybrid material. However, as reported by Faccioli et al.[27], the presence of the M-O-M signals in the hybrid materials can confirm the presence of the unaltered oxocluster structure, since these signals could not be detected after the hydrolysis of the inorganic core. The Raman spectra of the catalysts recovered after the catalytic tests are reported in Figure S35 – S39.

Conclusions

In this work, we successfully synthesized a series of nanosized hybrid organic-inorganic materials by incorporating Ti- (**Ti$_4$**, **Ti$_6$**) and bimetallic Ti-Zr- (**Ti$_2$Zr$_4$**, **Ti$_4$Zr$_2$**) oxoclusters, along with a reference Zr- (**Zr$_4$**) oxocluster, into a PMMA matrix via a photoactivated free-radical copolymerization in direct miniemulsion droplets. The synthesis yielded spherical nanoparticles which were characterized by FT-IR, Raman, TGA, and SEM.

Afterwards, the materials were tested as heterogeneous catalysts for the oxidation of methyl p-tolyl sulfide to the corresponding sulfoxide and sulfone using H_2O_2. The catalyses revealed that all hybrid nanoparticles were catalytically active. Notably, the monometallic Ti-based catalysts, **Ti$_4$**-20 and **Ti$_6$**-20, exhibited superior performance, achieving near-quantitative conversion and high selectivity towards the sulfone with higher initial rates, outperforming also previously reported heterogeneous systems based on Zr- or Hf- oxoclusters embedded into bulk polymers[20] (eventually including fluorinated co-monomers[18]) or nanoparticles.[28] Within this scenario, environmental applications in the field of oxidative desulfurization (ODS) of fuels, for which conversion of sulfides to sulfones is crucial, can be envisaged.[20]

To further improve the knowledge of the catalytic properties of oxocluster-based hybrid materials, we tested them also for the oxidation of benzyl alcohol, as an example of primary alcohol oxidation, and cyclooctene, as an example of alkene oxidation. As for the case of the sulfide oxidation, also in these cases the Ti-based catalysts resulted to be the most active in terms of conversion and rate, though in this case the catalytic performances were much lower than for the oxidation of methyl p-tolyl sulfide.

On one side, we attributed the high activity of the **Ti$_4$**-20 hybrid material to its high swelling degree in the reaction solvent, which may facilitate the access of reaction substrates to the Ti cations within the PMMA matrix. On the other side, the results of DFT calculations indicate that both **Ti$_4$**-OOH and **Zr$_4$**-OOH can form, but with a different geometry of coordination and with the Ti-OOH complex being less stable and, therefore, likely more reactive than the Zr-OOH complexes.

In summary, this research shows the successful synthesis of Ti-, Zr, and Ti-Zr-oxocluster-based hybrid nanoparticles as heterogeneous catalysts for H_2O_2-mediated oxidation reactions. In particular, we present the novel application of Ti-oxocluster-based hybrid materials as highly active catalysts for the oxidation of methyl p-tolyl sulfide, highlighting their potential use as catalysts for the oxidation of a broader range of organic substrates. All these findings provide a crucial starting point for future developments in sustainable catalysis using H_2O_2 as an oxidant and oxocluster-based hybrid materials as alternative catalysts.

Acknowledgments

References

(1)   Kickelbick, G. Hybrid Materials – Past, Present and Future. *Hybrid Materials* **2014**, *1* (1). https://doi.org/10.2478/hyma-2014-0001.
(2)   Kickelbick, G. *Hybrid Materials: Synthesis, Characterization, and Applications*, 1st reprint.; Wiley - VCH: Weinheim, 2007.
(3)   Gross, S. Oxocluster-Reinforced Organic–Inorganic Hybrid Materials: Effect of Transition Metal Oxoclusters on Structural and Functional Properties. *J. Mater. Chem.* **2011**, *21* (40), 15853–15861. https://doi.org/10.1039/C1JM10579E.
(4)   *Functional Hybrid Materials*; Gómez-Romero, P., Sanchez, C., Eds.; Wiley-VCH: Weinheim, 2004.

(5)   Ayandele, E.; Sarkar, B.; Alexandridis, P. Polyhedral Oligomeric Silsesquioxane (POSS)-Containing Polymer Nanocomposites. *Nanomaterials* **2012**, *2* (4), 445–475. https://doi.org/10.3390/nano2040445.

(6)   Cordes, D. B.; Lickiss, P. D.; Rataboul, F. Recent Developments in the Chemistry of Cubic Polyhedral Oligosilsesquioxanes. *Chem. Rev.* **2010**, *110* (4), 2081–2173. https://doi.org/10.1021/cr900201r.

(7)   Carraro, M.; Sandei, L.; Sartorel, A.; Scorrano, G.; Bonchio, M. Hybrid Polyoxotungstates as Second-Generation POM-Based Catalysts for Microwave-Assisted H_2O_2 Activation. *Org. Lett.* **2006**, *8* (17), 3671–3674. https://doi.org/10.1021/ol061197o.

(8)   Qi, W.; Wu, L. Polyoxometalate/Polymer Hybrid Materials: Fabrication and Properties: Polyoxometalate/Polymer Hybrid Materials. *Polym. Int.* **2009**, *58* (11), 1217–1225. https://doi.org/10.1002/pi.2654.

(9)   Proust, A.; Matt, B.; Villanneau, R.; Guillemot, G.; Gouzerh, P.; Izzet, G. Functionalization and Post-Functionalization: A Step towards Polyoxometalate-Based Materials. *Chem. Soc. Rev.* **2012**, *41* (22), 7605. https://doi.org/10.1039/c2cs35119f.

(10) Schubert, U. Cluster-Based Inorganic–Organic Hybrid Materials. *Chem. Soc. Rev.* **2011**, *40* (2), 575–582. https://doi.org/10.1039/C0CS00009D.

(11) Carraro, M.; Gross, S. Hybrid Materials Based on the Embedding of Organically Modified Transition Metal Oxoclusters or Polyoxometalates into Polymers for Functional Applications: A Review. *Materials* **2014**, *7* (5), 3956–3989. https://doi.org/10.3390/ma7053956.

(12) Schubert, U. Inorganic-Organic Hybrid Polymers Based on Surface-Modified Metal Oxide Clusters. *Macromol. Symp.* **2008**, *267* (1), 1–8. https://doi.org/10.1002/masy.200850701.

(13) Schubert, U. Titanium-Oxo Clusters with Bi- and Tridentate Organic Ligands: Gradual Evolution of the Structures from Small to Big. *Chemistry A European J* **2021**, *27* (44), 11239–11256. https://doi.org/10.1002/chem.202101287.

(14) Schubert, U. Polymers Reinforced by Covalently Bonded Inorganic Clusters. *Chem. Mater.* **2001**, *13* (10), 3487–3494. https://doi.org/10.1021/cm001258r.

(15) Trimmel, G.; Moraru, B.; Gross, S.; Di Noto, V.; Schubert, U. Cross-Linking of Poly(Methyl Methacrylate) by Oxozirconate and Oxotitanate Clusters. *Macromolecular Symposia* **2001**, *175* (1), 357–366. https://doi.org/10.1002/1521-3900(200110)175:1<357::AID-MASY357>3.0.CO;2-D.

(16) Kickelbick, G. Concepts for the Incorporation of Inorganic Building Blocks into Organic Polymers on a Nanoscale. *Progress in Polymer Science* **2003**, *28* (1), 83–114. https://doi.org/10.1016/S0079-6700(02)00019-9.

(17) Vendrame, D.; Bragaggia, G.; Carraro, M.; Gross, S. Metal Oxocluster-Based Organic–Inorganic Hybrid Materials: From Design Principles to Applications. *Chem. Mater.* **2024**. https://doi.org/10.1021/acs.chemmater.4c01141.

(18) Bragaggia, G.; Beghetto, A.; Bassato, F.; Reichenbächer, R.; Dolcet, P.; Carraro, M.; Gross, S. Tuning the Activity of a Hybrid Polymer–Oxocluster Catalyst: A Composition—Selectivity Correlation. *Polymers* **2021**, *13* (19), 3268. https://doi.org/10.3390/polym13193268.

(19) Trimmel, G.; Gross, S.; Kickelbick, G.; Schubert, U. Swelling Behavior and Thermal Stability of Poly(Methylmethacrylate) Crosslinked by the Oxozirconium Cluster Zr4O2(Methacrylate)12. *Applied Organometallic Chemistry* **2001**, *15* (5), 401–406. https://doi.org/10.1002/aoc.161.

(20) Vigolo, M.; Borsacchi, S.; Sorarù, A.; Geppi, M.; Smarsly, B. M.; Dolcet, P.; Rizzato, S.; Carraro, M.; Gross, S. Engineering of Oxoclusters-Reinforced Polymeric Materials with Application as Heterogeneous Oxydesulfurization Catalysts. *Applied Catalysis B: Environmental* **2016**, *182*, 636–644. https://doi.org/10.1016/j.apcatb.2015.10.008.

(21) Conte, V.; Di Furia, F.; Licini, G. Liquid Phase Oxidation Reactions by Peroxides in the Presence of Vanadium Complexes. *Applied Catalysis A: General* **1997**, *157* (1–2), 335–361. https://doi.org/10.1016/S0926-860X(97)00023-9.

(22) Antonova, N. S.; Carbó, J. J.; Kortz, U.; Kholdeeva, O. A.; Poblet, J. M. Mechanistic Insights into Alkene Epoxidation with H_2O_2 by Ti- and Other TM-Containing Polyoxometalates: Role of the Metal Nature and Coordination Environment. *J. Am. Chem. Soc.* **2010**, *132* (21), 7488–7497. https://doi.org/10.1021/ja1023157.

(23) Lane, B. S.; Burgess, K. Metal-Catalyzed Epoxidations of Alkenes with Hydrogen Peroxide. *Chem. Rev.* **2003**, *103* (7), 2457–2474. https://doi.org/10.1021/cr020471z.

(24) Noyori, R.; Aoki, M.; Sato, K. Green Oxidation with Aqueous Hydrogen Peroxide. *Chem. Commun.* **2003**, No. 16, 1977–1986. https://doi.org/10.1039/B303160H.

(25) Kaczorowska, K.; Kolarska, Z.; Mitka, K.; Kowalski, P. Oxidation of Sulfides to Sulfoxides. Part 2: Oxidation by Hydrogen Peroxide. *Tetrahedron* **2005**, *61* (35), 8315–8327. https://doi.org/10.1016/j.tet.2005.05.044.

(26) Jahier, C.; Mal, S. S.; Kortz, U.; Nlate, S. Dendritic Zirconium-Peroxotungstosilicate Hybrids: Synthesis, Characterization, and Use as Recoverable and Reusable Sulfide Oxidation Catalysts. *Eur J Inorg Chem* **2010**, *2010* (10), 1559–1566. https://doi.org/10.1002/ejic.200901141.

(27) Faccioli, F.; Bauer, M.; Pedron, D.; Sorarù, A.; Carraro, M.; Gross, S. Hydrolytic Stability and Hydrogen Peroxide Activation of Zirconium-Based Oxoclusters. *European Journal of Inorganic Chemistry* **2015**, *2015* (2), 210–225. https://doi.org/10.1002/ejic.201402767.

(28) Benedetti, C.; Cazzolaro, A.; Carraro, M.; Graf, R.; Landfester, K.; Gross, S.; Muñoz-Espí, R. Dual Role of Zirconium Oxoclusters in Hybrid Nanoparticles: Cross-Linkers and Catalytic Sites. *ACS Appl. Mater. Interfaces* **2016**, *8* (39), 26275–26284. https://doi.org/10.1021/acsami.6b07023.

(29) Landfester, K. Miniemulsion Polymerization and the Structure of Polymer and Hybrid Nanoparticles. *Angewandte Chemie International Edition* **2009**, *48* (25), 4488–4507. https://doi.org/10.1002/anie.200900723.

(30) Hood, M. A.; Mari, M.; Muñoz-Espí, R. Synthetic Strategies in the Preparation of Polymer/Inorganic Hybrid Nanoparticles. *Materials* **2014**, *7* (5), 4057–4087. https://doi.org/10.3390/ma7054057.

(31) Pablico, M. H.; Mertzman, J. E.; Japp, E. A.; Boncher, W. L.; Nishida, M.; Van Keuren, E.; Lofland, S. E.; Dollahon, N.; Rubinson, J. F.; Holman, K. T.; Stoll, S. L. Miniemulsion Synthesis of Metal–Oxo Cluster Containing Copolymer Nanobeads. *Langmuir* **2011**, *27* (20), 12575–12584. https://doi.org/10.1021/la2029774.

(32) Fischer, V.; Lieberwirth, I.; Jakob, G.; Landfester, K.; Muñoz-Espí, R. Metal Oxide/Polymer Hybrid Nanoparticles with Versatile Functionality Prepared by Controlled Surface Crystallization. *Advanced Functional Materials* **2013**, *23* (4), 451–466. https://doi.org/10.1002/adfm.201201839.

(33) Mari, M.; Müller, B.; Landfester, K.; Muñoz-Espí, R. Ceria/Polymer Hybrid Nanoparticles as Efficient Catalysts for the Hydration of Nitriles to Amides. *ACS Appl. Mater. Interfaces* **2015**, 7 (20), 10727–10733. https://doi.org/10.1021/acsami.5b01847.

(34) Benedetti, C.; Flouda, P.; Antonello, A.; Rosenauer, C.; Pérez-Pla, F. F.; Landfester, K.; Gross, S.; Muñoz-Espí, R. Zirconium Oxocluster/Polymer Hybrid Nanoparticles Prepared by Photoactivated Miniemulsion Copolymerization. *Nanotechnology* **2017**, *28* (36), 365603. https://doi.org/10.1088/1361-6528/aa7b6d.

(35) Mba, M.; Prins, L. J.; Zonta, C.; Cametti, M.; Valkonen, A.; Rissanen, K.; Licini, G. Ti(IV)-Amino Triphenolate Complexes as Effective Catalysts for Sulfoxidation. *Dalton Trans.* **2010**, *39* (31), 7384–7392. https://doi.org/10.1039/C0DT00228C.

(36) Sawada, Y.; Matsumoto, K.; Kondo, S.; Watanabe, H.; Ozawa, T.; Suzuki, K.; Saito, B.; Katsuki, T. Titanium–Salan-Catalyzed Asymmetric Epoxidation with Aqueous Hydrogen Peroxide as the Oxidant. *Angewandte Chemie International Edition* **2006**, *45* (21), 3478–3480. https://doi.org/10.1002/anie.200600636.

(37) Kholdeeva, O. A. Hydrogen Peroxide Activation over TiIV: What Have We Learned from Studies on Ti-Containing Polyoxometalates? *European Journal of Inorganic Chemistry* **2013**, *2013* (10–11), 1595–1605. https://doi.org/10.1002/ejic.201201396.

(38) Moraru, B.; Hüsing, N.; Kickelbick, G.; Schubert, U.; Fratzl, P.; Peterlik, H. Inorganic−Organic Hybrid Polymers by Polymerization of Methacrylate- or Acrylate-Substituted Oxotitanium Clusters with Methyl Methacrylate or Methacrylic Acid. *Chem. Mater.* **2002**, *14* (6), 2732–2740. https://doi.org/10.1021/cm021113f.

(39) Moraru, B.; Kickelbick, G.; Schubert, U. Methacrylate-Substituted Mixed-Metal Clusters Derived from Zigzag Chains of [ZrO8]/[ZrO7] and [TiO6] Polyhedra. *European Journal of Inorganic Chemistry* **2001**, *2001* (5), 1295–1301. https://doi.org/10.1002/1099-0682(200105)2001:5<1295::AID-EJIC1295>3.0.CO;2-Z.

(40) Frisch, M. J.; Trucks, G. W.; Schlegel, H. B.; Scuseria, G. E.; Robb, M. A.; Cheeseman, J. R.; Scalmani, G.; Barone, V.; Petersson, G. A.; Nakatsuji, H.; Li, X.; Caricato, M.; Marenich, A. V.; Bloino, J.; Janesko, B. G.; Gomperts, R.; Mennucci, B.; Hratchian, H. P.; Ortiz, J. V.; Izmaylov, A. F.; Sonnenberg, J. L.; Williams; Ding, F.; Lipparini, F.; Egidi, F.; Goings, J.; Peng, B.; Petrone, A.; Henderson, T.; Ranasinghe, D.; Zakrzewski, V. G.; Gao, J.; Rega, N.; Zheng, G.; Liang, W.; Hada, M.; Ehara, M.; Toyota, K.; Fukuda, R.; Hasegawa, J.; Ishida, M.; Nakajima, T.; Honda, Y.; Kitao, O.; Nakai, H.; Vreven, T.; Throssell, K.; Montgomery Jr., J. A.; Peralta, J. E.; Ogliaro, F.; Bearpark, M. J.; Heyd, J. J.; Brothers, E. N.; Kudin, K. N.; Staroverov, V. N.; Keith, T. A.; Kobayashi, R.; Normand, J.; Raghavachari, K.; Rendell, A. P.; Burant, J. C.; Iyengar, S. S.; Tomasi, J.; Cossi, M.; Millam, J. M.; Klene, M.; Adamo, C.; Cammi, R.; Ochterski, J. W.; Martin, R. L.; Morokuma, K.; Farkas, O.; Foresman, J. B.; Fox, D. J. Gaussian 16 Rev. C.01, 2016.

(41) Kreutzer, J.; Blaha, P.; Schubert, U. Assessment of Different Basis Sets and DFT Functionals for the Calculation of Structural Parameters, Vibrational Modes and Ligand Binding Energies of Zr4O2(Carboxylate)12 Clusters. *Computational and Theoretical Chemistry* **2016**, *1084*, 162–168. https://doi.org/10.1016/j.comptc.2016.03.030.

(42) Perdew, J. P.; Burke, K.; Ernzerhof, M. Generalized Gradient Approximation Made Simple. *Phys. Rev. Lett.* **1996**, *77* (18), 3865–3868. https://doi.org/10.1103/PhysRevLett.77.3865.

(43) Perdew, J. P.; Burke, K.; Ernzerhof, M. Generalized Gradient Approximation Made Simple. *Phys. Rev. Lett.* **1997**, *78* (7), 1396–1396. https://doi.org/10.1103/PhysRevLett.78.1396.

(44) Adamo, C.; Barone, V. Toward Reliable Density Functional Methods without Adjustable Parameters: The PBE0 Model. *The Journal of Chemical Physics* **1999**, *110* (13), 6158–6170. https://doi.org/10.1063/1.478522.

(45) Pritchard, B. P.; Altarawy, D.; Didier, B.; Gibson, T. D.; Windus, T. L. New Basis Set Exchange: An Open, Up-to-Date Resource for the Molecular Sciences Community. *J. Chem. Inf. Model.* **2019**, *59* (11), 4814–4820. https://doi.org/10.1021/acs.jcim.9b00725.

(46) Tomasi, J.; Mennucci, B.; Cammi, R. Quantum Mechanical Continuum Solvation Models. *Chem. Rev.* **2005**, *105* (8), 2999–3094. https://doi.org/10.1021/cr9904009.

(47) Mennucci, B. Polarizable Continuum Model. *WIREs Comput Mol Sci* **2012**, *2* (3), 386–404. https://doi.org/10.1002/wcms.1086.

(48) Allen, F. H. The Cambridge Structural Database: A Quarter of a Million Crystal Structures and Rising. *Acta Cryst B* **2002**, *58* (3), 380–388. https://doi.org/10.1107/S0108768102003890.

(49) Faccioli, F.; Bauer, M.; Pedron, D.; Sorarù, A.; Carraro, M.; Gross, S. Hydrolytic Stability and Hydrogen Peroxide Activation of Zirconium-Based Oxoclusters. *European Journal of Inorganic Chemistry* **2015**, *2015* (2), 210–225. https://doi.org/10.1002/ejic.201402767.

(50) Graziola, F.; Girardi, F.; Bauer, M.; Di Maggio, R.; Rovezzi, M.; Bertagnolli, H.; Sada, C.; Rossetto, G.; Gross, S. UV-Photopolymerisation of Poly(Methyl Methacrylate)-Based Inorganic–Organic Hybrid Coatings and Bulk Samples Reinforced with Methacrylate-Modified Zirconium Oxocluster. *Polymer* **2008**, *49* (20), 4332–4343. https://doi.org/10.1016/j.polymer.2008.08.005.

(51) Cerón-Carrasco, J. P.; Jacquemin, D.; Laurence, C.; Planchat, A.; Reichardt, C.; Sraïdi, K. Solvent Polarity Scales: Determination of New ET(30) Values for 84 Organic Solvents. *Journal of Physical Organic Chemistry* **2014**, *27* (6), 512–518. https://doi.org/10.1002/poc.3293.

(52) Gamelas, C. A.; Lourenço, T.; da Costa, A. P.; Simplício, A. L.; Royo, B.; Romão, C. C. Selective and Mild Oxidation of Sulfides to Sulfoxides or Sulfones Using H2O2 and Cp′Mo(CO)3Cl as Catalysts. *Tetrahedron Letters* **2008**, *49* (32), 4708–4712. https://doi.org/10.1016/j.tetlet.2008.05.126.

(53) Jeyakumar, K.; Chand, D. K. Selective Oxidation of Sulfides to Sulfoxides and Sulfones at Room Temperature Using H2O2 and a Mo(VI) Salt as Catalyst. *Tetrahedron Letters* **2006**, *47* (27), 4573–4576. https://doi.org/10.1016/j.tetlet.2006.04.153.

(54) Sato, K.; Hyodo, M.; Aoki, M.; Zheng, X.-Q.; Noyori, R. Oxidation of Sulfides to Sulfoxides and Sulfones with 30% Hydrogen Peroxide under Organic Solvent- and Halogen-Free Conditions. *Tetrahedron* **2001**, *57* (13), 2469–2476. https://doi.org/10.1016/S0040-4020(01)00068-0.

(55) Al-Maksoud, W.; Daniele, S.; Sorokin, A. B. Practical Oxidation of Sulfides to Sulfones by H2O2 Catalysed by Titanium Catalyst. *Green Chem.* **2008**, *10* (4), 447–451. https://doi.org/10.1039/B717696A.

(56) Bahrami, K. Selective Oxidation of Sulfides to Sulfoxides and Sulfones Using Hydrogen Peroxide (H2O2) in the Presence of Zirconium Tetrachloride. *Tetrahedron Letters* **2006**, *47* (12), 2009–2012. https://doi.org/10.1016/j.tetlet.2006.01.051.

(57) Garay-Ruiz, D.; Zonta, C.; Lovat, S.; González-Fabra, J.; Bo, C.; Licini, G. Elucidating Sulfide Activation Mode in Metal-Catalyzed Sulfoxidation Reactivity. *Inorg. Chem.* **2022**, *61* (10), 4494–4501. https://doi.org/10.1021/acs.inorgchem.2c00037.

(58) Lin, W.; Frei, H. Photochemical and FT-IR Probing of the Active Site of Hydrogen Peroxide in Ti Silicalite Sieve. *J. Am. Chem. Soc.* **2002**, *124* (31), 9292–9298. https://doi.org/10.1021/ja012477w.

(59) Van den Eynden, D.; Pokratath, R.; De Roo, J. Nonaqueous Chemistry of Group 4 Oxo Clusters and Colloidal Metal Oxide Nanocrystals. *Chem. Rev.* **2022**, *122* (11), 10538–10572. https://doi.org/10.1021/acs.chemrev.1c01008.

(60) Sheldon, R. A.; Arends, I. W. C. E.; ten Brink, G.-J.; Dijksman, A. Green, Catalytic Oxidations of Alcohols. *Acc. Chem. Res.* **2002**, *35* (9), 774–781. https://doi.org/10.1021/ar010075n.

(61) Davis, S. E.; Ide, M. S.; Davis, R. J. Selective Oxidation of Alcohols and Aldehydes over Supported Metal Nanoparticles. *Green Chem.* **2012**, *15* (1), 17–45. https://doi.org/10.1039/C2GC36441G.

(62) Ciriminna, R.; Pandarus, V.; Béland, F.; Xu, Y.-J.; Pagliaro, M. Heterogeneously Catalyzed Alcohol Oxidation for the Fine Chemical Industry. *Org. Process Res. Dev.* **2015**, *19* (11), 1554–1558. https://doi.org/10.1021/acs.oprd.5b00204.

(63) Venturello, C.; Alneri, E.; Ricci, M. A New, Effective Catalytic System for Epoxidation of Olefins by Hydrogen Peroxide under Phase-Transfer Conditions. *J. Org. Chem.* **1983**, *48* (21), 3831–3833. https://doi.org/10.1021/jo00169a052.

(64) Sheldon, R. A.; Arends, I. W. C. E.; Hanefeld, U. *Green Chemistry and Catalysis*, 1st ed.; Wiley, 2007. https://doi.org/10.1002/9783527611003.

(65) Maksimchuk, N. V.; Marikovskaya, S. M.; Larionov, K. P.; Evtushok, V. Yu.; Yanshole, V. V.; Antonov, A. A.; Kholdeeva, O. A. Effect of the Polyanion Structure on the Mechanism of Alcohol Oxidation with H2O2 Catalyzed by Zr-Substituted Polyoxotungstates. *Inorg. Chem.* **2024**, *63* (39), 18043–18057. https://doi.org/10.1021/acs.inorgchem.4c02641.

(66) Ni, Z.; Lv, H.; Yang, G. Recent Advances of Ti/Zr-Substituted Polyoxometalates: From Structural Diversity to Functional Applications. *Molecules* **2022**, *27* (24), 8799. https://doi.org/10.3390/molecules27248799.

(67) Maksimchuk, N. V.; Kholdeeva, O. A. H2O2-Based Selective Oxidations Catalyzed by Supported Polyoxometalates: Recent Advances. *Catalysts* **2023**, *13* (2), 360. https://doi.org/10.3390/catal13020360.

(68) Kickelbick, G.; Feth, M. P.; Bertagnolli, H.; Puchberger, M.; Holzinger, D.; Gross, S. Formation of Organically Surface-Modified Metal Oxo Clusters from Carboxylic Acids and Metal Alkoxides: A Mechanistic Study. *J. Chem. Soc., Dalton Trans.* **2002**, No. 20, 3892–3898. https://doi.org/10.1039/B207994A.

DIPARTIMENTO DI SCIENZE CHIMICHE
DEPARTMENT OF CHEMICAL SCIENCES

UNIVERSITÀ DEGLI STUDI DI PADOVA

Data availability statement

The data supporting this article have been included as part of the Supplementary Information.

Sincerely,

Padova, 28/04/2025

Silvia Gross

Mauro Carraro